https://doi.org/10.1038/s44355-024-00001-z

Alterations of the peptidomic composition of peripheral plasma after portal hypertension correction by transjugular intrahepatic portosystemic shunt

Check for updates

Giulia Ilaria Bagarolo[1,8], Shruti Bhargava[1,8], Robert Schierwagen[2], Wenyi Gu[2,3], Vera Jankowski[1], Josefin Soppert[1], Emona Barzakova[4], Federica Cascone[1], Olaf Tyc[3], Christiane Kuhl[4], Heidi Noels[1,5], Jonel Trebicka[2,6] & Joachim Jankowski[1,5,7]

Portal hypertension develops in patients with advanced chronic liver diseases (CLD), especially cirrhosis and is associated with complications, such as gastrointestinal bleeding and ascites resulting in high mortality. The transjugular intrahepatic portosystemic shunt (TIPS) is a treatment option for portal hypertension, aiming to decrease portal venous pressure by establishing an artificial passage for blood from the gastrointestinal tract to the liver vein. This study focuses on the differences in the molecular composition of plasma samples from patients with portal hypertension before and after TIPS intervention to identify and characterise potential mediators influencing gut-liver cross-talk. The plasma of 23 patients displaying advanced CLD with portal hypertension was collected from peripheral veins before and after TIPS treatment and analysed using a well-established non-targeted chromatography-mass spectrometric (LC-MS) approach. Sialomucin core protein 24(CD164)(160–180), meckelin(99-118), Histone-lysine N-methyltransferase(MLL3)(3019-3045) and transient receptor potential cation channel subfamily V member 5(TRPV5)(614-630) were identified to be downregulated after the TIPS treatment. In addition, the metabolites 3-carboxy-4-methyl-5-propyl-2-furanpropionic acid (CMPF), uric acid, dopamine, homoarginine, leucylproline and 5-methyluridine were significantly decreased after TIPS, whereas one yet unidentified low molecular-weight metabolite showed an increase after the medical procedure. In conclusion, these substances are novel potential biomarkers for portal hypertension in patients with CLD, with mechanistic clues of involvement in regulating pathological gut-liver cross-talk.

Portal hypertension is a frequent complication of liver cirrhosis[1], defined by a more than 6 mmHg pressure gradient between the portal vein and the vena cava[2]. Portal hypertension causes complications like (a) gastroesophageal varices, associated with a high risk of variceal bleeding[3–5], (b) ascites, resulting in abdominal distension[4] and (c) high risk for bacterial infections, resulting in bacterial peritonitis and/or pneumonia[4].

Portal hypertension impacts the bidirectional, biomolecule-mediated gut and liver relationship. Portal hypertension, accompanied by dysbiosis and CLD, increases intestinal barrier permeability and translocates bacterial

[1]Institute of Molecular Cardiovascular Research, University Hospital RWTH Aachen, Aachen, Germany. [2]Department of Internal Medicine B, University of Münster, Münster, Germany. [3]Translational Hepatology, Department of Internal Medicine I, Goethe University Frankfurt, Frankfurt, Germany. [4]Department of Diagnostic and Interventional Radiology, University Hospital RWTH Aachen, Aachen, Germany. [5]Cardiovascular Research Institute Maastricht (CARIM), University of Maastricht, Maastricht, The Netherlands. [6]European Foundation for the Study of Chronic Failure, EFCLIF, Barcelona, Spain. [7]Aachen-Maastricht Institute for Cardiorenal Disease (AMICARE), University Hospital RWTH Aachen, Aachen, Germany. [8]These authors contributed equally: Giulia Ilaria Bagarolo, Shruti Bhargava.
e-mail: jjankowski@ukaachen.de

components and biomolecules, potentially inducing systemic and low-grade inflammation[6]. Gut-derived mediators, such as tryptophan and indole derivates, access the liver through the portal vein blood and affect the hepatic status[7]. In addition, systemic circulation influences the interaction between the intestine and the liver by transferring metabolites from the liver to the intestine via capillary diffusion[8].

Management of portal hypertension complications involves pharmacological treatment with non-selective β-blockers (NSBB) like carvedilol[9]. However, the most effective and established clinical procedure for portal hypertension management is a transjugular intrahepatic portosystemic shunt (TIPS) between the hepatic and portal vein[10,11], thereby decreasing the portal pressure and avoiding portal hypertension-associated complications[12].

Since methods like transient elastography or magnetic resonance cannot be employed on certain patients[13,14] where it is not feasible to measure hepatic venous pressure gradient[15], there is a strong need for alternative non-invasive, broadly applicable diagnostic biomarkers for portal hypertension.

Plasma biomolecule concentrations are promising diagnostic markers for early detection of portal hypertension. Peptidomics is a proteomics-derived omics technique based on e.g. liquid chromatography-mass-spectrometry as an efficient method for both targeted and non-targeted peptide identification in diseases[16–18].

Therefore, this study used a non-targeted peptidomics approach to identify low molecular weight biomolecules dysregulated in the plasma of patients affected by CLD and portal hypertension as potential biomarkers and potential mediators of pathological gut-liver cross-talk. The cohort considered in this study was selected to investigate the portal hypertension changes after TIPS, and the plasma samples were collected within 7–14 days after TIPS, representing the typical recovery window for TIPS intervention[19].

Results

Patients' characteristics

A total of 23 patients (65% males), who suffered from portal hypertension and underwent TIPS procedures, were included in this study. Patients' ages ranged from 34 to 81 years old, with an average value of 55.7 (±12.5). The mean body mass index of the patients was 26.3 (±4.6), and the mean heart rate was 76.1 bpm (±12.5). Biochemistry evaluation of blood collected on the first visit was performed as shown in Table 1 and represents the clinical image of advanced CLD with liver dysfunction based on Child-Pugh scores, inflammation based on C reactive protein and portal hypertension based on the portal and systemic hemodynamic parameters. Demographic data like age, gender, and BMI was registered. The patients diagnosed with liver cirrhosis ($n = 13$) were i) alcohol-related liver cirrhosis ($n = 10$) (absent from alcohol consumption $n = 5$), ii) active hepatitis C ($n = 1$), iii) Metabolic dysfunction-associated steatotic liver disease (MASLD) ($n = 1$) and iv) autoimmune hepatitis (AIH) ($n = 1$). Ten patients were without a diagnosis of cirrhosis, including four with hepatic sinusoidal obstruction syndrome, three with Budd-Chiari syndrome, and three with unknown aetiology. Child-Pugh score before intervention was 7.5 (±1.9), indicating moderately impaired hepatic function[20], and the score significantly decreased after TIPS to 6.1 (±1.1). Nine patients were classified in class A of Child-Pugh scores with 5–6 points, signifying a good hepatic function; nine patients in class B of Child-Pugh scores with 7–9 points, signifying moderately impaired hepatic function; and one patient in class C of Child-Pugh scores with 10–15 points signifying advanced hepatic dysfunction before TIPS and improved to 14 patients in class A and six patients in B class after TIPS treatment.

MELD score went from 9.9 (± 4.6) before to 9.1 (± 4.1) after TIPS treatment. The MELD-Na score ranged from 11.7 (± 5.5) before to 10.5 (± 5.5) after the TIPS intervention. The mean portal hepatic venous pressure gradient (PHPG) before TIPS treatment was 17.6 mmHg (± 6.9) and 8.8 mmHg(± 3.7) after the intervention. Portal pressure (mmHg) decreased from 22.2 (± 6.9) to 16 (± 5.1) after the intervention. The systolic and diastolic blood pressure before and after TIPS was not significantly different, with a change from 114.4 ± 12.3 to 112.4 ± 17.4 and from 69.6 ± 10.8 to 65.2 ± 10.1, respectively. Patients also showed lower levels of bilirubin, alanine aminotransferase[21], aspartate transaminase (AST), gamma-glutamyl transferase (γ-GT), alkaline phosphatase (A.P.), inflammatory marker C-reactive protein (CRP) and urea after the TIPS treatment as summarised in Table 1. Before the TIPS procedure, patients with or without cirrhosis had similar Child-Pugh scores, MELD scores, and portal and systemic hemodynamic parameters but different MELD-Na scores, among other characteristics, as summarised in Supplemental material Table s1.

Peptidomic analyses of plasma samples

A characteristic reversed-phase chromatogram of an EDTA plasma sample isolated from peripheral veins is shown in Fig. 1C, and the corresponding 'total ion chromatogram' of the mass spectrometric analysis of plasma from a patient before the TIPS treatment is shown in Fig. 1D. The corresponding 'total ion chromatogram' from the plasma of the same patient after TIPS is shown in Fig. 1E.

Identification of differentially expressed molecular features by limma statistics

By bucketing, unique molecular features within the plasma samples were identified, and mass-signal intensities were collected in buckets defined by R.T. and m/z with a retention time tolerance of 0.3 min and mass-spectrometric tolerance of 0.4 Da. The final analysis included 79 normally distributed molecular features. The differentially expressed molecular features were ranked by their adjusted p values and B values before and after TIPS treatment.

Eleven significant differentially occurring molecular features in the peripheral vein before vs. after TIPS were identified (adjusted p value ≤ 0.05). These molecular features, their logFC, and adjusted p values are given in Table 2. The molecular features measured after TIPS treatment showed a logFC 5-fold lower than their respective logFC before TIPS treatment, except the molecular feature showed a positive logFC, indicating an increase after TIPS treatment.

The mass signal intensities of the molecular features at 863.4 m/z, 943.0 m/z, 951.4 m/z and 1045.8 m/z within the peripheral vein plasma significantly decreased after TIPS intervention (Fig. 2). The identical effect was observed for the biomolecules with mass signal intensities at 153.0 m/z, 169.0 m/z, 241.0 m/z, 187.8 m/z, 229.0 m/z and 259.0 m/z (Fig. 3). The molecular feature at 154.2 m/z showed an increased mass-signal intensity after the TIPS treatment, but was not identified based on the low molecular weight(supplemental material Fig. S1). The Supplemental material Table S2 reports the percentages of zero intensity values in the cohorts.

Correlation analyses

The baseline molecular feature at 154.2 m/z positively correlated with the PHPG after TIPS treatment (Fig. 4A). The baseline of the molecular feature at 187.8 m/z negatively correlated with leucocytes after the TIPS treatment (Fig. 4A). Interestingly, the baseline value before TIPS insertion at 951.4 m/z negatively correlated with PHPG after treatment (Fig. 4A), while the increase after TIPS insertion (Δ) showed a strong significant positive correlation (Fig. 4B). Additionally, 943.0 m/z at baseline correlated positively with serum creatinine (Fig. 4A), while the changes correlated negatively (Fig. 4B). Moreover, the feature at 863.4 m/z showed a negative correlation with a marker for liver damage alanine aminotransferase (ALT) after TIPS treatment (Fig. 4A).

Sequencing mediators

The underlying amino acid sequences of the molecular features were identified by MALDI-TOF/TOF mass-spectrometry (Ultraflex-III TOF/TOF, Bruker-Daltonic, Germany), Orbitrap mass-spectrometry (Thermo-Fisher, Germany) as well as LC-ESI mass-spectrometry (HCT, Bruker-Daltonics, Germany). Figure 5A shows a characteristic HCT mass-spectrum of the molecular feature at 169.0 m/z. The underlying mediator was fragmented by MS/MS, resulting in the identification of uric acid, as shown in Fig. 5B.

Table 1 | Characteristics of the 23 patients before and after TIPS placement.

Variable	Before TIPS	After TIPS	*p* value
	(*n* = 23)		
Age	57 (34–81)		
Male	13 (59.1%)		
BMI	25.6 (15.5–32.9)	26.9 (16.4–34.7)	0.086
Liver cirrhosis	13 (61.9%)		
Aetiology of cirrhosis			
Alcohol	9 (42.9%)		
Alcohol and alpha-1 antitrypsin deficiency	1 (4.8%)		
HCV	1 (4.8%)		
Metabolic dysfunction-associated steatotic liver disease	1 (4.8%)		
Auto-immune hepatitis	1 (4.8%)		
Aetiology of non-cirrhosis with portal hypertension			
Hepatic sinusoidal obstruction syndrome	4 (17.4%)		
Budd-Chiari syndrome	3 (15.8%)		
Cryptogenic	3 (15.8%)		
History of decompensations			
Ascites paracentesis	4 (17.4%)		
Hepatorenal syndrom	2 (9.6%)		
Variceal bleeding	9 (42.9%)		
Hepatic encephalopathy	1 (4.8%)		
Bacterial infection	1 (4.8%)		
Portal vein thrombosis	5 (21.7%)	4 (17.4%)	
Bacterial infections	6 (31.6%)	1 (4.8%)	
Acute-on-chronic liver failure	6 (31.6%)	1 (4.8%)	
TIPS indication			
Acute Variceal bleeding failure of control	6 (31.6%)		
Refractory/recurrent ascites	10 (52.6%)		
Both indications	3 (15.8%)		
Other indications	4 (17.4%)		
TIPS stent type: Viatorr (covered)	23 (100%)		
Year of TIPS: 2014/2015/2016/2017	2 (9.1%)/3 (13.6%)/10 (45.5%)/ 7 (31.8%)		
Scores			
Child-Pugh	8 (5–11)	6 (5–8)	0.001
Child class (A/B/C)	9 (47.4%)/ 9(47.4%)/ 1(5.3%)	14 (70.0%)/ 6(30.0%)/ 0(0.0%)	
MELD	9 (6–22)	11 (6–22)	0.267
MELD-Na	11 (6–25)	6 (6–22)	0.143
Portal and systemic hemodynamic parameters			
PHPG (mmHg)	20 (5–25)	9 (3–18)	<0.0001
Portal pressure (mmHg)	23.5 (15–30)	15.5 (7–25)	<0.0001
Systolic arterial pressure (mmHg)	119 (100–150)	112 (85–152)	0.562
Diastolic arterial pressure (mmHg)	72 (43–90)	65 (50–90)	0.510
Laboratory			
Leucocytes (g/L)	6.93 (2.34–17.5)	6.13 (2.08–10.12)	0.047
Hb (g/dL)	9.6 (7.1–13)	12.2 (8.1–16.9)	<0.0001
Platelets (g/L)	129 (30–320)	139 (42–478)	0.378
INR	1.1 (0.9–1.6)	1.2 (1–2.7)	0.273
Bilirubin (mg/dL)[a]	1.13 (0.31–8.7)	1.29 (0.28–54)	0.289
ALT (Units/L)	34 (11–148)	30 (16–50)	0.382
AST (Units/L)[a]	44 (11–242)	46 (22–119)	0.629
γ-GT (Units/L)	137.5 (28–770)	113.5 (24–484)	0.276
AP (Units/L)[a]	143.5 (66–486)	145 (90–333)	0.842
Albumin (g/L)	31.45 (13.6–45.7)	35.7 (21.4–62.9)	0.012
Serum creatinine (mg/dL)	0.9 (0.59–6)	0.95 (0.48–2.6)	0.289
Sodium (mmol/L)	140 (126–147)	141 (133–142)	0.602
Urea (mg/dL)[a]	42 (14–126)	27.6 (7–68)	0.046
CRP (ml/L)[a]	17.5 (1.7–91.9)	2.935 (0.55–32.8)	0.069
Treatment			
Beta blocker	9 (42.9%)	10 (47.6%)	0.761
Diuretics	20 (90.9%)	19 (86.4%)	0.635
Antibiotics	9 (39.1%)	4 (17.4%)	

Continuous variables are showed with median (minimum–maximum). Categorical variables are showed with number (percentage). The percentages are corrected for missing values for each parameter.

BMI body mass index, *MELD* model for end-stage liver disease, *MELD-Na* model for end-stage liver disease, *PHPG* portal hepatic venous pressure gradient, *Hb* haemoglobin, *INR* internal normalised ratio, *ALT* alanine aminotransferase, *AST* aspartate transaminase, *γ-GT* serum glutamyl-transpeptidase, *AP* alkaline phosphatase, *CRP* C-reactive protein. Of note: beta-blockers are traditional NSBB/carvedilol.

[a]Indicates markers outside of the reference values.

The peptide with the m/z ratio 863.4 originates from the protein ′Histone-lysine N-methyltransferase′ (MLL3) (3019–3045). The peptide with an m/z ratio of 943 was found to be a Meckelin peptide (99–118), and the peptide with an m/z ratio of 951.4 is cleaved from the ′Transient receptor potential cation channel subfamily V member 5′ (TRPV5). The m/z ratio of 1045.8 corresponded to amino acids 160–180 of sialomucin core protein 24 (CD164) (Table 3). The Table 3 lists metabolites identified by LC-ESI-MS/MS and literature mining, which led to the structure identification of dopamine (m/z ratio 153), uric acid (m/z ratio 169), homoarginine (m/z ratio 187.8), leucylproline (m/z ratio 229), 3-carboxy-4-methyl-5-propyl-2-furanpropionic acid (CMPF) (m/z ratio 241) and 5-methyluridine (m/z ratio 259).

Discussion

Portal hypertension impacts the physiology and pathophysiology of the gut and the liver through the gut-liver axis, leading to venous congestion in the intestine and disrupting the intestinal barrier. Since the knowledge of gut-liver cross-talk is limited, an increasing number of studies are focusing on analysing the role of gut-liver cross-talk in chronic inflammatory diseases[22]. This includes the investigation of gut dysbiosis in liver diseases like MASLD, alcohol-related liver disease, liver cirrhosis and hepatic carcinogenesis[23,24], as well as the development of novel therapeutic strategies targeting the gut microbiota in liver diseases[25]. By analysing the plasma of patients displaying portal hypertension, biomarkers were identified as diagnostic tools and therapeutic mediators contributing to understanding the gut and liver cross-talk. We could not analyse the correlation of the identified peptides with post-TIPS hepatic encephalopathy as in our cohort, only one patient developed post-TIPS hepatic encephalopathy. The low incidence of post-TIPS hepatic encephalopathy might be related to our cohort's use of covered TIPS.

Using an untargeted peptidomics approach, we identified novel potential mediators differentially occurring in the blood of patients who underwent TIPS treatment. We developed peptidomics data analyses to discover and determine new biomarkers[16,17] and identify novel peptides to be used in prevention and

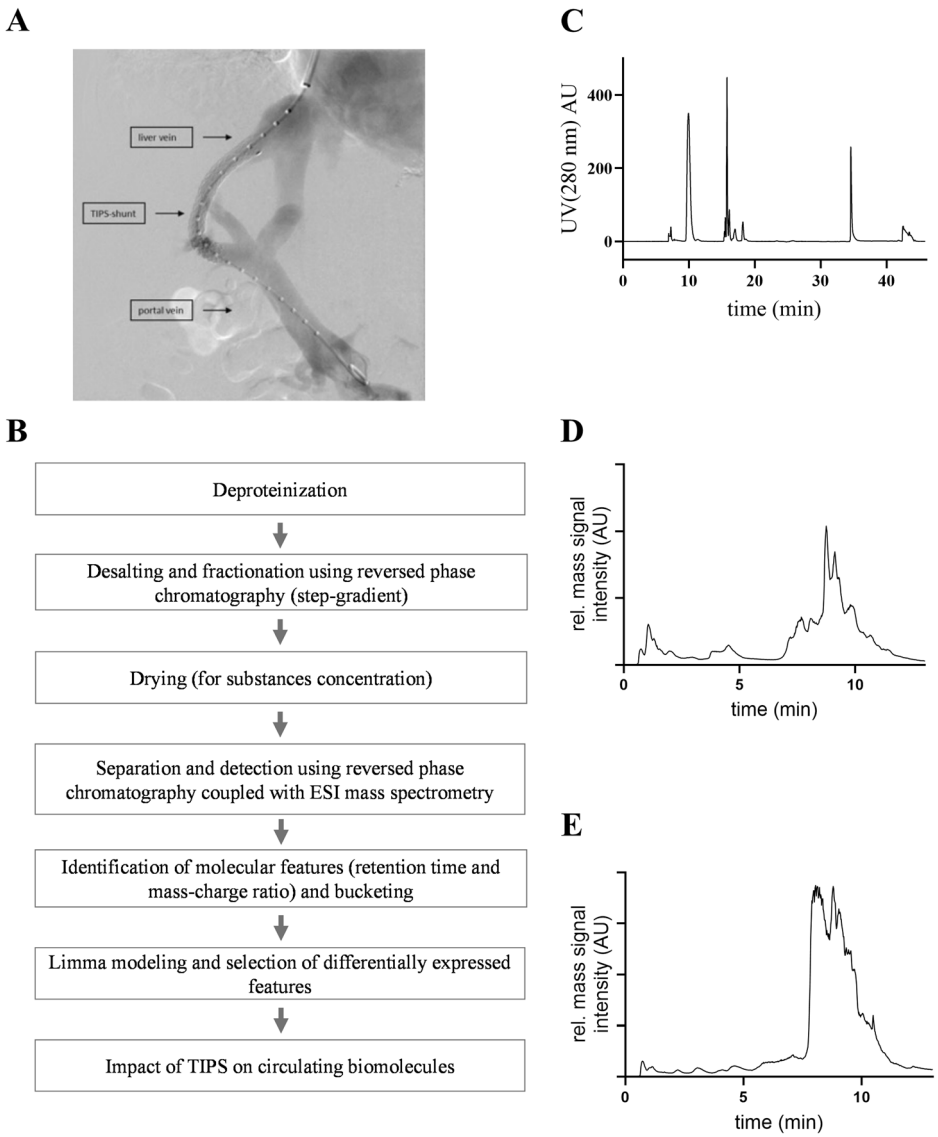


Fig. 1 | TIPS procedure, blood sample collection of patients suffering from displaying portal hypertension, reverse-phase chromatography, and electrospray ionisation mass-spectrometry for isolating mediators involved in gut–liver cross-talk. A TIPS procedure connecting the hepatic and portal veins to reduce the portal pressure. **B** Workflow of sample preparation for mass spectrometric analyses and biomolecule identification. **C** Desalting and fractionation of peptides via HPLC (time of the run 46 min, gradient: 0–10 min: 100% A; 10–20 min: 80% A - 20% B; 20–30 min: 60% A - 40% B; 30–38 min: 0% A - 100% B; 38-46 min: 100% A - 0% B; eluent A = TFA (0.1% v/v), eluent B = ethanol (80% v/v); U.V. absorbance = λ_{280} nm). Total ion chromatogram of a peripheral vein sample from a patient before TIPS (**D**) and after TIPS (**E**). *A.U. arbitrary units.*

prediction models[26]. The peptidomics approach focused on mediators with a significantly different expression before vs after TIPS treatment. The peptidomics data were analysed using 'limma' statistics[27,28] and t-statistics, identifying ten molecular features that decreased after TIPS treatment and increased intensity of one molecular feature. The Δs of four molecular markers (187.8, 863.4, 943.0, 951.4 each *m/z*) correlated with leucocytes amount, ALT, serum creatinine and PHPG, demonstrating the potential of the novel biomolecules in the contest of the portal hypertension diagnosis and treatment.

Four of these ten biomolecules were identified and sequenced as peptides (Table 3). The literature points to the potential mechanisms by which the parent proteins of these peptides impact portal hypertension or liver regeneration (summarised in Fig. 6A):

The origin protein of peptide MLL3 (3019–3045) regulates metabolic processes and the hepatic circadian control of bile acid homoeostasis[29]. MLL3 is involved in fatty liver development[30] and MASLD pathology by methylation of histone 3 forming H3K4me3, which interacts with the promoters of PPARγ resulting in increased de novo lipogenesis in hepatocytes leading to MASLD[24,31].

The parent protein of Meckelin (99–118) negatively regulates the canonical Wnt signalling, and activates the non-canonical cascade stimulated by Wnt5A[32], a regulator of β-catenin signalling and hepatocyte proliferation[33]. The Wnt5a/Frizzled-2 axis suppresses β-catenin signalling in

Table 2 | List of molecular features identified to be differentially expressed in peripheral vein plasma samples before vs. after TIPS.

Molecular feature	LogFC	Adjusted *p* value
1.85 min: 153.0 m/z	−11.85	0.001
3.35 min: 154.2 m/z	7.88	0.041
1.25 min: 169.0 m/z	−7.79	0.012
4.55 min: 187.8 m/z	−12.67	0.003
1.25 min: 229.0 m/z	−8.59	0.012
1.55 min: 241.0 m/z	−5.60	0.041
1.25 min: 259.0 m/z	−8.12	0.012
9.05 min: 863.4 m/z	−8.22	0.041
2.15 min: 943.0 m/z	−9.13	0.012
10.85 min: 951.4 m/z	−7.16	0.026
1.85 min: 1045.8 m/z	−5.52	0.044

The molecular features with relative logFC and adjusted *p* values are shown. Significant differences were identified through the test limma. Negative values indicate a decrease in the peripheral vein after vs. before TIPS; positive values indicate an increase in the peripheral vein after vs. before TIPS. *LogFC* log2-fold-change.

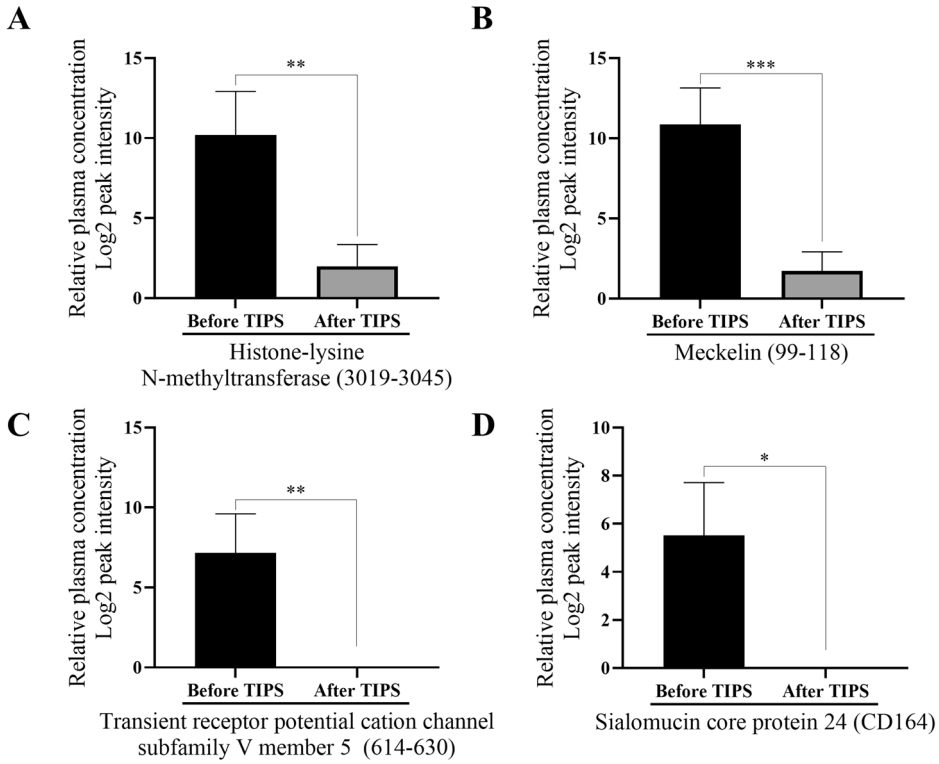


Fig. 2 | Differential molecular feature expression of identified peptides in peripheral blood before and after TIPS treatment. Bar plots quantifying the molecular features 863.4 m/z (**A**), 943.0 m/z (**B**), 951.4 m/z (**C**) and 1045.8 m/z (**D**) in peripheral vein blood before vs. after TIPS treatment of patients with portal hypertension ($n = 17$ before TIPS, $n = 20$ after TIPS). Data are shown as mean ± SEM. $^{*}p \leq 0.05$, $^{**}p \leq 0.005$, $^{***}p \leq 0.0005$.

hepatocytes, contributing to the conclusion of the liver regeneration process. Therefore, the reduction in Meckelin after the TIPS procedure might reduce the stimulation of WNT5A, promoting liver regeneration and overcoming the injury of portal hypertension.

The peptide TRPV5 (614–630) was cleaved from a protein, regulating Ca^{2+} reabsorption in the kidney and intestine[34–36]. Deranged hepatocyte intracellular Ca^{2+} homoeostasis promotes the progression of NASLD[24,37,38], but the impact on portal hypertension or liver disorders has not yet been identified until now.

The parent protein of the peptide CD164 (160–180) is involved in haematopoiesis[39], with high expression in the pathological context of portal hypertension before TIPS treatment and is increasingly expressed in liver tissue in pro-inflammatory, high-cholesterol conditions[40]. In addition, CD164 is a downstream functional effector of 'Insulin-Like Growth Factor 2 mRNA-Binding Protein 3' (IGF2BP3)[41], which is overexpressed in acute liver injury[42]. CD164 activates the CXCR4 axis, promoting inflammation and migration of cells[41]. Therefore, the downregulation of CD164 after the TIPS procedure is concurrent with the reduction of pathological stress on the liver cells caused by portal hypertension.

Our findings show the downregulation of MLL3 (3019–3045), Meckelin (99–118), TRPV5 (614–630), and CD164 (160–180) are, therefore, the first step towards establishing these peptides as biomarkers of portal hypertension.

The remaining mediators are derived from gut and liver metabolism and/or previously related to liver (patho)physiology (Table 3). Since the concentration of these mediators decreased after TIPS, they are correlated to portal hypertension and might act as biomarkers for early, non-invasive diagnostics. The mechanisms through which these metabolites influence portal hypertension or liver regeneration are shown in Fig. 6B.

Approximately 50% of dopamine is produced in the gastrointestinal tract and is involved in cell immunity regulation as well as in suppressing autoimmune hepatitis[43]. Liver cirrhosis inhibits dopamine synthesis due to a 'false' dopaminergic transmission resulting from increased availability of aromatic neurotransmitters precursors[44] and increases natriuresis[45], leading to an expected increase in endogenous dopamine production after TIPS. Dopamine is also therapeutic against acute liver failure by inhibiting NLRP3 inflammasome activation and enhancing hepatic regeneration[46]. In addition, agonism of dopamine receptor D1 hinders the nuclear localisation of YAP/TAZ, which is causal for acute liver injury. Therefore, binding dopamine to its receptors is an essential step in liver regeneration and could account for the lower levels of dopamine post-TIPS treatment. However, the exact mechanism by which dopamine impacts portal hypertension is not known.

The liver produces uric acid and induces hepatic steatosis through mitochondrial oxidative stress production hereby[47]. Higher serum levels of uric acid are associated with a higher probability of developing MASLD[24,48]. Uric acid leads to monosodium urate crystals forming, which activate the NLRP3 inflammasome, promoting acute liver injury. The underlying mechanism involved is activating the Toll-like receptor 2/4-Myd88 pathway and increased transcriptional levels of pro-IL-1β through the NF-κB pathway[49]. Therefore, a decrease in uric acid coincides with an expected reduction in liver disorders after the TIPS treatment.

Homoarginine is synthesised by the liver[50,51] and is an inhibitor of alkaline phosphatases[52,53]. Abnormal liver biomarkers such as Alanine aminotransferase, Aspartate-amino transferase, fibrosis (Fib-4) score, liver fat content, and cholinesterase are related to greater circulating hArg concentrations in the general population[50], supporting our finding that reduction in portal hypertension leads to a reduction of circulating homoarginine levels.

The present study shows that Leucylproline concentrations are higher in plasma in patients affected by MASLD-cirrhosis and decreased after TIPS treatment. Branched-chain amino acids (BCAA) such as leucine and proline have been reported to be decreased in liver cirrhosis[44,54], however, in chronic liver diseases, an increase of BCAAs has been observed[55]. The utilisation of BCAA-rich medications has demonstrated favourable outcomes among individuals diagnosed with cirrhosis[55]. However, the exact mechanisms by which BCAAs play a role in portal hypertension are unknown. Moreover, the identified dipeptide Leucylproline might have a different mechanism of action than individual BCAAs.

CMPF is suggested as a MASLD prediction marker[24,56] since high plasma levels of CMPF negatively correlate with lipid metabolism. CMPF promotes the production of reactive oxygen species, lipid peroxidation, and intracellular iron accumulation[57]. In this context, detecting a reduced CMPF concentration by the TIPS treatment is highly relevant for patients with liver diseases. Last but not least, the metabolite 5-methyluridine was detected in

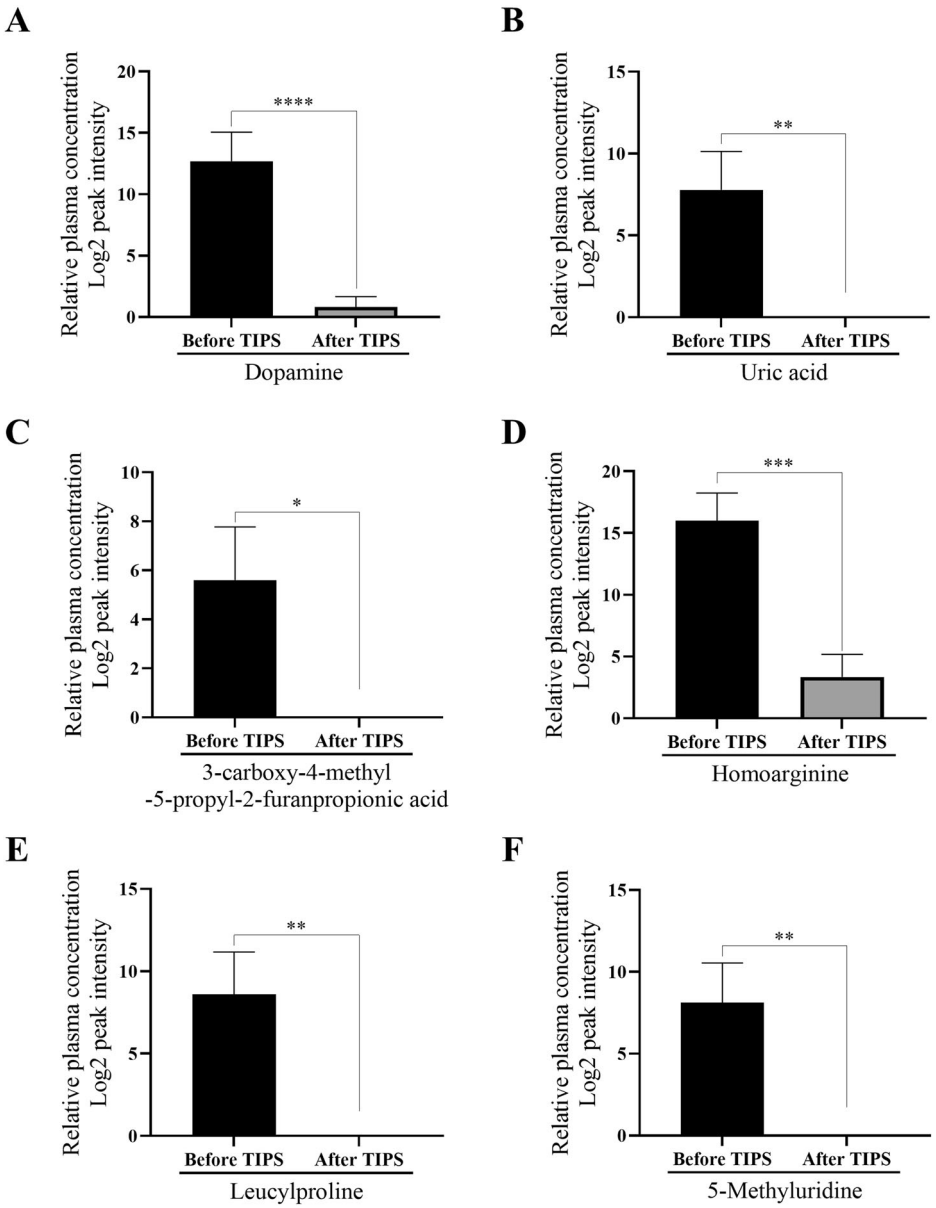


Fig. 3 | Differential molecular feature expression of identified metabolites in peripheral blood before and after TIPS treatment. Bar plots quantifying the molecular features 153 m/z (**A**), 169 m/z (**B**), 187.8 m/z (**C**), 229 m/z (**D**), 241 m/z (**E**) and 259 m/z (**F**) in peripheral vein blood before vs. after TIPS treatment of patients with portal hypertension ($n = 17$ before TIPS, $n = 20$ after TIPS). Data are shown as mean ± SEM. $^{*}p \le 0.05$, $^{**}p \le 0.001$, $^{***}p \le 0.0005$, $^{****}p \le 0.00005$.

humans[58] and *E. Coli*[59] but has not been so far linked to liver cirrhosis, MASLD, NASH or portal hypertension[24]. The results of the present studies provide interesting approaches for investigating these interactions.

Indeed, our study has some limitations. First of all, this is a retrospective cohort with a limited number of patients included with different etiologies, including cirrhosis and non-cirrhosis with portal hypertension. However, we have paired plasma samples in these patients before TIPS insertion and during follow-up visits. Although the patients were included over four years, all patients received the same type of TIPS stent, limiting our results' bias. However, we still believe samples from patients with severe portal hypertension are valuable. The related peptides could offer insights into the potential markers and mechanisms of different outcomes and events after the TIPS procedure since the TIPS procedure needs experienced radiologists and hepatologists. Of course, further prospective studies are required to validate our findings.

In summary, eleven mediators were differentially expressed in the plasma of peripheral veins after TIPS treatment and require further in vivo validation based on the solid evidence from published data linking these mediators to liver regeneration, MASLD and liver cirrhosis, among other pathophysiological pathways. The current study demonstrates that these mediators could play a role in the gut-liver axis organ crosstalk pathophysiology. Moreover, while the current findings suggest a potential role for these mediators in gut-liver axis organ crosstalk, further experiments and clinical investigations are imperative to substantiate their significance and elucidate their precise mechanisms of action.

Methods

Description of the patient cohort

A total of 23 patients from the observational NEPTUN ('Non-invasive Evaluation Programme for TIPS and Follow-Up Network'; clinicaltrials.gov identifier: NCT03628807) with a pressure gradient between the portal vein and vena cava above 6 mmHg, and undergoing a TIPS treatment using VIATORR® Controlled Expansion (VCX) type were included in the study (Fig. 1A, Table 1). The study design is a retrospective cohort, and the study was approved by the local ethics committee of the University of Bonn (029/13). All patients signed informed written consent following the Declaration of Helsinki.

200 µL EDTA plasma was collected from peripheral veins before and after TIPS treatment. The peripheral plasma samples before TIPS at baseline were taken during the TIPS procedure when patients were under analgesia.

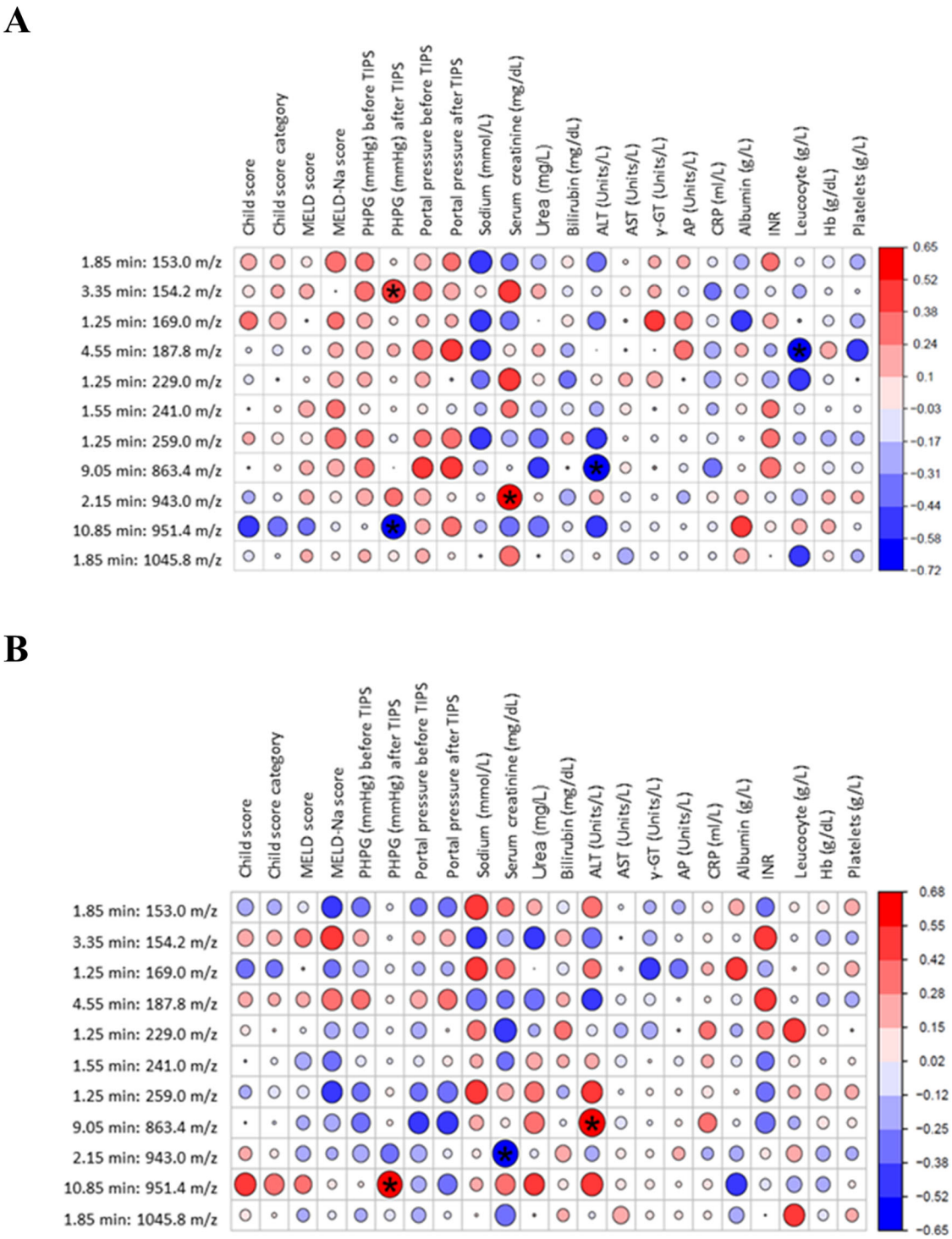


Fig. 4 | Pearson correlations of the eleven molecular features from baseline to follow-up and clinical characteristics. A shows the correlation between the baseline molecular features and the clinical markers. **B** shows the correlation between molecular features after TIPS vs clinical markers. The *P* value is reported as $*p < 0.05$; the darker the colour of the circle represented in the figure, the stronger the correlation.

Therefore, there were no significant differences between blood sampling and TIPS procedure in the patients of our cohort. Paired samples of the patients were taken at regular follow-up visits after TIPS insertion. Plasma was subsequently processed and stored at −80 °C until analysis. The portal-hepatic pressure gradient was measured during the TIPS procedure according to the guideline, which involves the insertion of a catheter into the hepatic vein and the portal vein with the guidance of the ultrasound. Portal and inferior vena cava pressures were measured to calculate the porto-hepatic pressure gradient pre- and post-TIPS insertion. Scores and classes to predict the outcome of portal hypertension in patients, such as 'Child-Pugh score', 'Child class and Model for End-Stage Liver Disease' (MELD) score, were collected, as well as the 'Model for End-Stage Liver Disease-Na' (MELD-Na).

Plasma sample preparation for chromatographic analysis

The plasma samples were defrosted and centrifuged at 956 g for 10 min at 4 °C. A total of 1 µg of Sar-Thr-angiotensin II (Sigma-Aldrich, Germany)

was added as an internal standard. Plasma proteins were denatured by adding perchloric acid 70% (PCA) with a ratio of 65 µL per mL of plasma. After centrifugation at 956 g for 10 min at 4 °C, the supernatant was transferred to a fresh tube and the pH was adjusted to a value ≥ 9.0 by adding potassium hydroxide (5 mol/L). Plasma samples were frozen at −20 °C for 24 h, thawed and centrifuged at 956 *g* for 10 min at 4 °C. The supernatant was collected, and the pH was adjusted to 7.0 ± 0.1 by adding PCA before proceeding with high-performance liquid chromatography.

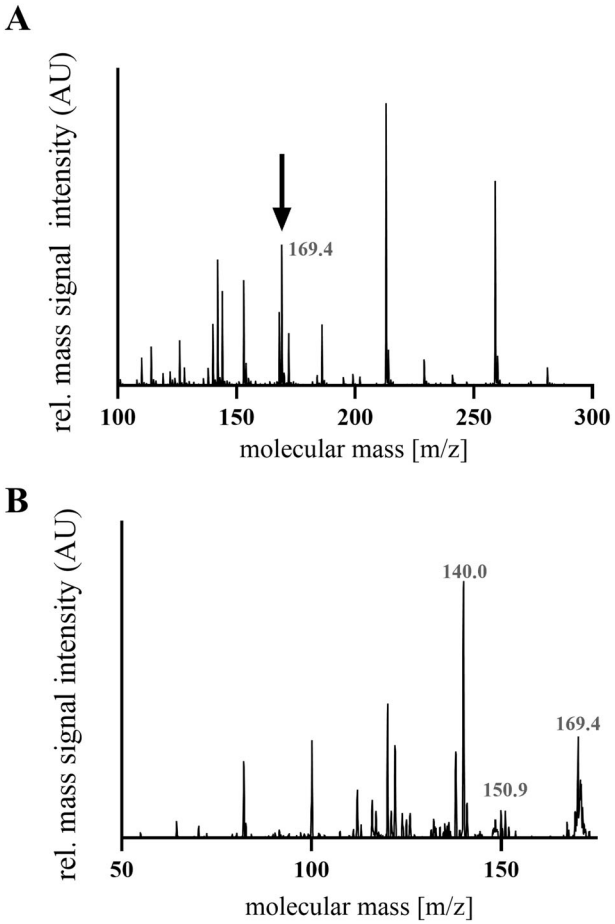


Fig. 5 | Detailed mass spectrum and fragmentation of molecular feature with mass signal 169.0. A Mass spectrum of the feature with m/z 169.0. **B** Representative MS/MS fragmentation of the molecular feature 169.0 m/z was identified as the metabolite uric acid.

High-performance liquid chromatography (HPLC)

The deproteinated plasma samples were diluted by adding 0.1% trifluoroacetic acid (TFA) and were fractionated by high-performance liquid chromatography (HPLC) by using a C^{18}-chromolith^{TM} reverse-phase chromatographic column (100 mm × 4.6 mm; Merck, Germany). TFA in water (0.1% v/v) was used as the polar solvent A, and hydrophobic solvent B was constituted by ethanol (80% v/v) in water, maintaining a flow rate of 1 mL/min for 46 min. The fractionation was performed by a gradient as follows: 0–10 min: 0% B, 10–20 min: 20% B, 20–30 min: 40% B, 30–38 min: 100% B, 38–46 min: 100% A and 0% B. The fractions were lyophilised with a freeze-drying technique by employing a Savant Speed Vac (SPD101B, Thermo Fisher Scientific, USA) and 'Refrigerated Vapor Trap' (Thermo Fisher Scientific, USA) after the chromatographic separation.

Liquid chromatography coupled with electrospray ionisation-mass-spectrometry (LC-ESI-MS) for peptide identification

The lyophilised samples were re-suspended in water and formic acid (0.1% v/v) in a total volume of 50 µL. The samples underwent fractionation by capillary-HPLC (Agilent 1200, Germany), employing a 'C^{18} SB Zorbax' column (150 × 0.5 mm, 5 µm, Agilent Technologies, Germany). Eluent A was formic acid (0.1% v/v), and eluent B was acetonitrile (99.9% v/v) (Thermo Fisher Scientific, Germany) with formic acid (0.1% v/v). The flow rate of the solvents was 60 µL/min for 22 min, and the temperature was stable at 50 °C. The re-suspended samples were fractioned by 0–2 min: 0% eluent B, 2–10 min: 0–30% B, 30–100% B, 13.5–15.5 min: 100% B, 15.5–16.0 min: 0–100% A and 100–0% B, and 16–22 min: 100% A and 0% B. The eluate obtained after the chromatographic separation was analysed with a high-capacity ion-trap (HCT) mass spectrometer (Bruker-Daltonics, Germany).

The mass analyser employed was used in the positive ion mode with a source temperature of 300 °C to detect the eluted mediator's molecular masses (*m/z*). The nebuliser gas was kept at 20 psi, and the dry gas flow was accustomed to 9 L/min. For the detection of compounds, the mass spectrometric accumulation time of the ion trap was set to 200 ms. The mass spectrometer was tuned in the wide-mode option on *m/z* 800 and operated in enhanced mode scanning for m/z between 100 and 1500. Data were acquired and processed with the software HyStar 3.2 (Bruker-Daltonics, Germany).

Table 3 | List of peptides and metabolites identified by MALDI-TOF/TOF mass-spectrometry and LC-ESI-MS/MS and list of metabolites identified by LC-ESI-MS/MS to be differentially expressed in peripheral blood before vs. after TIPS.

R.T. min—m/z	Sequence	Parent protein and amino acid position
9.05 min: 863.4 m/z	HSLGTGKPATQTGPQTSQSGTSSMSG	Histone-lysine N-methyltransferase MLL3 (3019-3045)
2.15 min: 943.0 m/z	KCPENMKGVTEDGWNCISCPSDLTAE	Meckelin (99-118)
10.85 min: 951.4 m/z	PRSGICGCEFGLGDRWF	Transient receptor potential cation channel subfamily V (614-630)
1.85 min: 1045.8 m/z	TFDAASFIGGIVLVLGVQAVI	Sialomucin core protein 24 (160-180)
	Chemical formula	Metabolite name
1.85 min: 153.0 m/z	$C_8H_{11}NO_2$	Dopamine
1.25 min: 169.0 m/z	$C_5H_4N_4O_3$	Uric acid
4.55 min: 187.8 m/z	$C_7H_{16}N_4O_2$	Homoarginine
1.25 min: 229.0 m/z	$C_{11}H_{20}N_2O_3$	Leucylproline
1.55 min: 241.0 m/z	$C_{12}H_{16}O_5$	3-carboxy-4-methyl-5-propyl-2-furanpropionic acid
1.25 min: 259.0 m/z	$C_{10}H_{14}N_2O_6$	5-Methyluridine

The molecular features in terms of R.T. and m/z are shown, followed by the sequence, name of the protein of origin and amino acid position; or followed by the molecular formula and the name of the metabolite.
RT retention time.

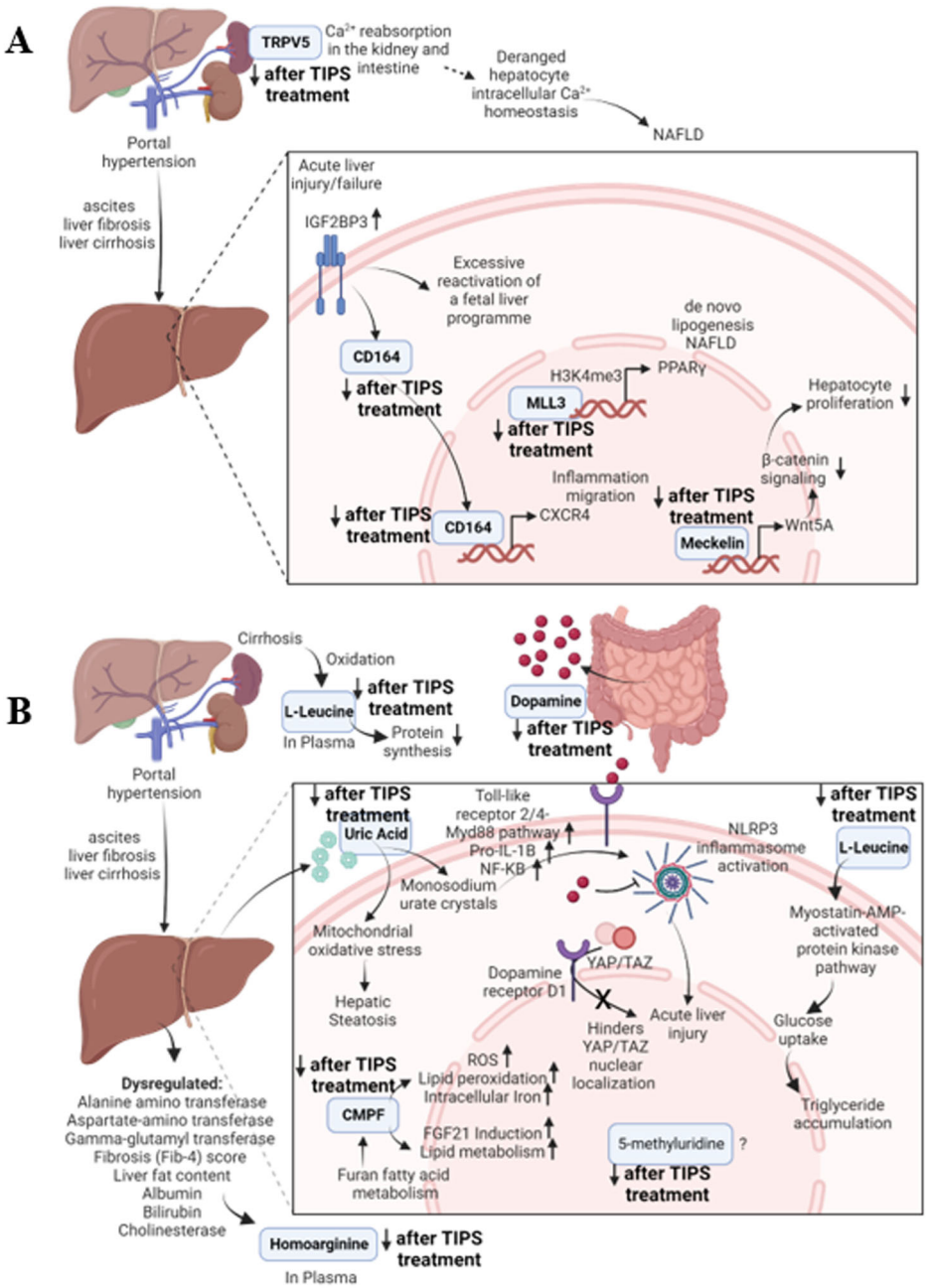


Fig. 6 | Mechanistic correlations of the identified features to gut-liver cross-talk. A Mechanisms by which the identified parent proteins might impact portal hypertension or liver regeneration. **B** Mechanisms by which the identified metabolites might impact portal hypertension or liver regeneration.

Data processing

Mass-spectrometry raw data were processed, and the molecular features were visualised through the mass-spectrometric software 'DataAnalysis 4.0' (Bruker-Daltonics, Germany). Specific molecular features were selected with the 'FindMolecularFeatures' (FMF) algorithm and were characterised by the retention time (R.T.), the m/z, and the intensity of the peak. The FMF algorithm was based on (i) signal-to-noise ratio (S/N), used for discriminating between noise and compound (used value: 2)[60] (ii) correlation coefficient threshold, which defines the minimal time correlation to combine peak clusters (used value: 0.79); (iii) minimum compound length, which specifies the number of spectra to determine a peak (used value: 10); (iv) smoothing width, to smooth out the chromatogram with the value of 2; and (v) background subtraction. The resulting data were transposed into a bucket table, characterising the features by their R.T., *m/z* and mass intensity. Similar compounds were bundled together with an R.T. tolerance of 0.3 min and m/z tolerance of 0.4, aiming at the reduction of size and complexity of the dataset, easing out the following statistical analyses. Features with more than 80% of zero values and were not unique regarding R.T. and *m/z*, were excluded from further analyses.

Statistical analyses

The bucketed data were statistically analysed using the RStudio open source software (RStudio Team, 2016. M.A., USA) and GraphPad Prism version (9.1.1 for Windows, GraphPad Software, CA, USA). The intensities of the molecular features were normalised by the internal standard, converted to $\log_2$ and tested for normal distribution. The 'limma'[61] was implemented in the RStudio workflow to fit the data to a linear model, with the function 'lmfit', followed by 'makeContrasts' and 'contrasts.fit'[61] to estimate the coefficients and standard errors for every contrast declared in the original model. The method' eBayes'[61] was used to identify differential abundances of the molecular features. A false discovery rate adjustment was performed, obtaining adjusted *p* values for multiple t-tests using the 'toptable' function and extracting the best-ranked molecular features. The statistical approach

analysed differences in log_2 intensities of the molecular features in samples before vs. after TIPS intervention.

Two sets of correlation analyses were performed to investigate whether the molecular features correlated with the CLD clinical markers. In the first set of correlations, the intensities of the molecular feature before TIPS were compared to the clinical markers, while for the second set of correlations, a delta was calculated by subtracting the mass-signal intensity after treatment from the intensity before treatment (Δ). The data were adjusted, and Pearson correlation analyses were performed using RStudio.

The unidentified molecular feature at 154.2 m/z was normally distributed, however, the other features were not normally distributed. Therefore, the molecular feature at 154.2 m/z was analysed with parametric tests and for all the other molecular features which were not normally distributed, nonparametric tests with Mann Whitney test as a post-hoc test were used for statistical analysis.

Identification of amino acid sequences of the molecular features

To investigate the amino acid sequences of the identified molecular features, 1 µL of the re-suspended samples and a matrix (α-4-hydroxycinnamic acid, 2.5 mg/mL) were applied on a Rapiflex plate support and analysed by employing a BrukerUltraflex-III TOF/TOF instrument (Bruker-Daltonic, Germany). MS/MS fragmentation was performed to fragment the molecular features, reconstruct the sequences using ions a, b and y, and align the results to the 'Mascot database' (Matrix Science Inc, Boston (M.A.), U.S.). Identification of low-weight molecular weight features was performed by MS/MS employing the LC-ESI mass-spectrometry (Bruker-Daltonics, Germany) followed by literature mining with open sources databases 'human metabolome database'[60] and 'PubChem'[18]. The workflow steps of sample preparation, data processing and analysis are shown in Fig. 1B.

Received: 17 February 2024; Accepted: 2 May 2024;
Published online: 10 June 2024

References

1. Iwakiri, Y. & Trebicka, J. Portal hypertension in cirrhosis: pathophysiological mechanisms and therapy. *JHEP Rep.* **3**, 100316, https://doi.org/10.1016/j.jhepr.2021.100316 (2021.
2. Berzigotti, A., Seijo, S., Reverter, E. & Bosch, J. Assessing portal hypertension in liver diseases. *Expert Rev. Gastroenterol. Hepatol.* **7**, 141–155 (2013).
3. Simonetto, D. A., Liu, M. & Kamath, P. S. Portal hypertension and related complications: diagnosis and management. *Mayo Clin Proc.* **94**, 714–726 (2019).
4. Toshikuni, N., Takuma, Y. & Tsutsumi, M. Management of gastroesophageal varices in cirrhotic patients: current status and future directions. *Ann. Hepatol.* **15**, 314–325 (2016).
5. Gu, W. et al. Trends and the course of liver cirrhosis and its complications in Germany: nationwide population-based study (2005 to 2018). *Lancet Reg. Health Eur.* **12**, 100240, https://doi.org/10.1016/j.lanepe.2021.100240 (2022).
6. Martel, J. et al. Gut barrier disruption and chronic disease. *Trends Endocrinol. Metab.* **33**, 247–265 (2022).
7. Agus, A., Clement, K. & Sokol, H. Gut microbiota-derived metabolites as central regulators in metabolic disorders. *Gut* **70**, 1174–1182 (2021).
8. Tripathi, A. et al. The gut-liver axis and the intersection with the microbiome. *Nat. Rev. Gastroenterol. Hepatol.* **15**, 397–411 (2018).
9. Schwarzer, R. et al. Carvedilol for reducing portal pressure in primary prophylaxis of variceal bleeding: a dose-response study. *Aliment Pharmacol. Ther.* **47**, 1162–1169 (2018).
10. Sauerbruch T., Schierwagen R., Trebicka J. Managing portal hypertension in patients with liver cirrhosis. *F1000Research* 2018;7 https://doi.org/10.12688/f1000research.13943.1.
11. Boyer, T. D. & Haskal, Z. J., American Association for the Study of Liver D. The role of transjugular intrahepatic portosystemic shunt (TIPS) in the management of portal hypertension: update 2009. *Hepatology* **51**, 306 (2010).
12. Rosch, J. & Keller, F. S. Transjugular intrahepatic portosystemic shunt: present status, comparison with endoscopic therapy and shunt surgery, and future prospectives. *World J. Surg.* **25**, 337–345 (2001).
13. Berzigotti, A. et al. Elastography, spleen size, and platelet count identify portal hypertension in patients with compensated cirrhosis. *Gastroenterology* **144**, 102–111.e1 (2013).
14. Castera, L., Pinzani, M. & Bosch, J. Non invasive evaluation of portal hypertension using transient elastography. *J. Hepatol.* **56**, 696–703 (2012).
15. Qi, X., Berzigotti, A., Cardenas, A. & Sarin, S. K. Emerging non-invasive approaches for diagnosis and monitoring of portal hypertension. *Lancet Gastroenterol. Hepatol.* **3**, 708–719 (2018).
16. Gajjala, P. R. et al. Novel plasma peptide markers involved in the pathology of CKD identified using mass spectrometric approach. *J. Mol. Med.* **97**, 1451–1463 (2019).
17. Gajjala, P. R. et al. Proteomic-biostatistic integrated approach for finding the underlying molecular determinants of hypertension in human plasma. *Hypertension* **70**, 412–419 (2017).
18. Schrader, M. & Selle, H. The process chain for peptidomic biomarker discovery. *Dis. Markers* **22**, 27–37 (2006).
19. Dariushnia, S. R. et al. Quality improvement guidelines for transjugular intrahepatic portosystemic shunts. *J. Vasc. Interv. Radiol.* **27**, 1–7 (2016).
20. Pugh, R. N., Murray-Lyon, I. M., Dawson, J. L., Pietroni, M. C. & Williams, R. Transection of the oesophagus for bleeding oesophageal varices. *Br. J. Surg.* **60**, 646–649 (1973).
21. Dietrich, T., Sharma, P., Walter, C., Weston, P. & Beck, J. The epidemiological evidence behind the association between periodontitis and incident atherosclerotic cardiovascular disease. *J. Clin. Periodontol.* **40**, S70–S84 (2013).
22. Atif, M., Warner, S. & Oo, Y. H. Linking the gut and liver: crosstalk between regulatory T cells and mucosa-associated invariant T cells. *Hepatol. Int.* **12**, 305–314 (2018).
23. Trebicka, J., Reiberger, T. & Laleman, W. Gut-liver axis links portal hypertension to acute-on-chronic liver failure. *Visc. Med.* **34**, 270–275 (2018).
24. Rinella, M. E. et al. A multisociety Delphi consensus statement on new fatty liver disease nomenclature. *J. Hepatol.* **79**, 1542–1556 (2023).
25. Trebicka, J., Bork, P., Krag, A. & Arumugam, M. Utilizing the gut microbiome in decompensated cirrhosis and acute-on-chronic liver failure. *Nat. Rev. Gastroenterol. Hepatol.* **18**, 167–180 (2021).
26. Wendt, R. et al. A urinary peptidomic profile predicts outcome in SARS-CoV-2-infected patients. *eClinicalMedicine* **36**, 100883, https://doi.org/10.1016/j.eclinm.2021.100883 (2021).
27. Kammers, K., Cole, R. N., Tiengwe, C. & Ruczinski, I. Detecting significant changes in protein abundance. *EuPA Open Proteom.* **7**, 11–19 (2015).
28. Dunkler, D., Sanchez-Cabo, F. & Heinze, G. Statistical analysis principles for Omics data. *Methods Mol. Biol.* **719**, 113–131 (2011).
29. Kim, D. H. et al. Crucial roles of mixed-lineage leukemia 3 and 4 as epigenetic switches of the hepatic circadian clock controlling bile acid homeostasis in mice. *Hepatology* **61**, 1012–1023 (2015).
30. Lee, S., Lee, J., Lee, S. K. & Lee, J. W. Activating signal cointegrator-2 is an essential adaptor to recruit histone H3 lysine 4 methyltransferases MLL3 and MLL4 to the liver X receptors. *Mol. Endocrinol.* **22**, 1312–1319 (2008).
31. Song, J. et al. Deficiency of peroxisomal NUDT7 stimulates de novo lipogenesis in hepatocytes. *iScience* **25**, 105135, https://doi.org/10.1016/j.isci.2022.105135 (2022).
32. Abdelhamed, Z. A. et al. The Meckel-Gruber syndrome protein TMEM67 controls basal body positioning and epithelial branching morphogenesis in mice via the non-canonical Wnt pathway. *Dis. Model Mech.* **8**, 527–541 (2015).

33. Yang, J. et al. WNT5A inhibits hepatocyte proliferation and concludes beta-catenin signaling in liver regeneration. *Am. J. Pathol.* **185**, 2194–2205 (2015).
34. de Groot, T., Bindels, R. J. & Hoenderop, J. G. TRPV5: an ingeniously controlled calcium channel. *Kidney Int.* **74**, 1241–1246 (2008).
35. Zhang, W., Na, T. & Peng, J. B. WNK3 positively regulates epithelial calcium channels TRPV5 and TRPV6 via a kinase-dependent pathway. *Am. J. Physiol. Renal. Physiol.* **295**, F1472–F1484 (2008).
36. Kirchhoff, P. & Geibel, J. P. Role of calcium and other trace elements in the gastrointestinal physiology. *World J. Gastroenterol.* **12**, 3229–3236 (2006).
37. Das, S. & Choudhuri, D. Calcium supplementation shows a hepatoprotective effect against high-fat diet by regulating oxidative-induced inflammatory response and lipogenesis activity in male rats. *J. Tradit. Complement. Med.* **10**, 511–519 (2020).
38. Ali, E. S., Rychkov, G. Y. & Barritt, G. J. Deranged hepatocyte intracellular Ca(2+) homeostasis and the progression of non-alcoholic fatty liver disease to hepatocellular carcinoma. *Cell Calcium* **82**, 102057, https://doi.org/10.1016/j.ceca.2019.102057 (2019).
39. Tang, J. et al. Inhibiting CD164 expression in colon cancer cell line HCT116 leads to reduced cancer cell proliferation, mobility, and metastasis in vitro and in vivo. *Cancer Investig.* **30**, 380–389 (2012).
40. Kleemann, R. et al. Atherosclerosis and liver inflammation induced by increased dietary cholesterol intake: a combined transcriptomics and metabolomics analysis. *Genome Biol.* **8**, R200 (2007).
41. Mancarella, C. et al. Insulin-like growth factor 2 mRNA-binding protein 3 modulates aggressiveness of ewing sarcoma by regulating the CD164-CXCR4 Axis. *Front. Oncol.* **10**, 994 (2020).
42. Hyun, J. et al. Dysregulated activation of fetal liver programme in acute liver failure. *Gut* **68**, 1076–1087 (2019).
43. Xue, R. et al. Peripheral dopamine controlled by gut microbes inhibits invariant natural killer T cell-mediated hepatitis. *Front. Immunol.* **9**, 2398 (2018).
44. Marrone, G. et al. Branched chain amino acids in hepatic encephalopathy and sarcopenia in liver cirrhosis: evidence and uncertainties. *World J. Gastroenterol.* **29**, 2905–2915 (2023).
45. Choi, M. R. et al. Renal dopaminergic system: pathophysiological implications and clinical perspectives. *World J. Nephrol.* **4**, 196–212 (2015).
46. Zhan, C. et al. A dopamine-precursor-based nanoprodrug for in-situ drug release and treatment of acute liver failure by inhibiting NLRP3 inflammasome and facilitating liver regeneration. *Biomaterials* **268**, 120573, https://doi.org/10.1016/j.biomaterials.2020.120573 (2021).
47. Lanaspa, M. A. et al. Uric acid induces hepatic steatosis by generation of mitochondrial oxidative stress: potential role in fructose-dependent and -independent fatty liver. *J. Biol. Chem.* **287**, 40732–40744 (2012).
48. Lee, J. W. et al. Serum uric acid as a predictor for the development of nonalcoholic fatty liver disease in apparently healthy subjects: a 5-year retrospective cohort study. *Gut Liver* **4**, 378–383 (2010).
49. Kushiyama, A. et al. Role of uric acid metabolism-related inflammation in the pathogenesis of metabolic syndrome components such as atherosclerosis and nonalcoholic steatohepatitis. *Mediators Inflamm.* **2016**, 8603164, https://doi.org/10.1155/2016/8603164 (2016).
50. Aghdassi, A. et al. The relationship between homoarginine and liver biomarkers: a combination of epidemiological and clinical studies. *Sci. Rep.* **13**, 5230 (2023).
51. Adams, S. et al. Novel biosynthesis, metabolism and physiological functions of L-homoarginine. *Curr. Protein Pept. Sci.* **20**, 184–193 (2019).
52. Pilz, S. et al. Association of homoarginine and methylarginines with liver dysfunction and mortality in chronic liver disease. *Amino Acids* **47**, 1817–1826 (2015).
53. Alvaro, D. et al. The function of alkaline phosphatase in the liver: regulation of intrahepatic biliary epithelium secretory activities in the rat. *Hepatology* **32**, 174–184 (2000).
54. Tajiri, K. & Shimizu, Y. Branched-chain amino acids in liver diseases. *Transl. Gastroenterol. Hepatol.* **3**, 47 (2018).
55. Lo E. K. K., et al. The emerging role of branched-chain amino acids in liver diseases. *Biomedicines*. **10**, https://doi.org/10.3390/biomedicines10061444 (2022).
56. Dai, J. et al. Serum 3-carboxy-4-methyl-5-propyl-2-furanpropanoic acid is associated with lipid profiles and might protect against non-alcoholic fatty liver disease in Chinese individuals. *J. Diabetes Investig.* **10**, 793–800 (2019).
57. Park, J. S. et al. 3-Carboxy-4-methyl-5-propyl-2-furanpropanoic acid (CMPF) induces cell death through ferroptosis and acts as a trigger of apoptosis in kidney cells. *Cell Death Dis.* **14**, 78 (2023).
58. Krawczyk, H. The stilbene derivatives, nucleosides, and nucleosides modified by stilbene derivatives. *Bioorg. Chem.* **90**, 103073 (2019).
59. Bjork, G. R. & Neidhardt, F. C. Physiological and biochemical studies on the function of 5-methyluridine in the transfer ribonucleic acid of Escherichia coli. *J. Bacteriol.* **124**, 99–111 (1975).
60. Wishart, D. S. et al. HMDB 5.0: the human metabolome database for 2022. *Nucleic Acids Res.* **50**, D622–D631 (2022).
61. Ritchie, M. E. et al. limma powers differential expression analyses for RNA-sequencing and microarray studies. *Nucleic Acids Res.* **43**, e47 (2015).

Acknowledgements

The authors are supported by grants from the German Research Foundation (DFG) (SFB/TRR 219 project-ID: 322900939; Project-ID 445703531 and SFB 1382 Project-ID 403224013), KFO 5011, COST Action CA21165 (Personalised medicine in chronic kidney disease: improved outcome based on Big Data (PerMediK)), as well as by the European Union's Horizon 2020 research and innovation programme under the Marie Skłodowska-Curie grant agreement No 764474 (CaReSyAn) and No 860329 (Strategy-CKD). This study was supported by the German Federal Ministry of Education and Research (BMBF) for the DEEP-HCC project, and by the Hessian Ministry of Higher Education, Research and the Arts (HMWK) for the ACLF-I cluster project. The MICROB-PREDICT (project ID 825694), DECISION (project ID 847949), GALAXY (project ID 668031), LIVERHOPE (project ID 731875), and IHMCSA (project ID 964590) projects have received funding from the European Union's Horizon 2020 research and innovation programme.

Author contributions

J.J. and S.B. designed research studies, G.I.B., F.C. and S.B. conducted experiments, G.I.B., W.G., V.J., J.S., E.B., C.K., O.T. and S.B. acquired data, G.I.B., O.T., C.K. and S.B. analysed data, R.S., H.N. and J.T. provided reagents, G.I.B., J.J. and S.B. wrote the manuscript.

Funding

Open Access funding enabled and organized by Projekt DEAL.

Competing interests

The authors declare no competing interests.

Additional information

Supplementary information The online version contains supplementary material available at https://doi.org/10.1038/s44355-024-00001-z.

Correspondence and requests for materials should be addressed to Joachim Jankowski.

Reprints and permissions information is available at http://www.nature.com/reprints

Publisher's note Springer Nature remains neutral with regard to jurisdictional claims in published maps and institutional affiliations.

Open Access This article is licensed under a Creative Commons Attribution 4.0 International License, which permits use, sharing, adaptation, distribution and reproduction in any medium or format, as long as you give appropriate credit to the original author(s) and the source, provide a link to the Creative Commons license, and indicate if changes were made. The images or other third party material in this article are included in the article's Creative Commons license, unless indicated otherwise in a credit line to the material. If material is not included in the article's Creative Commons license and your intended use is not permitted by statutory regulation or exceeds the permitted use, you will need to obtain permission directly from the copyright holder. To view a copy of this license, visit http://creativecommons.org/licenses/by/4.0/.

© The Author(s) 2024